

Kirsten P. Stone, Desiree Wanders, Manda Orgeron, Cory C. Cortez, and Thomas W. Gettys



# Mechanisms of Increased In Vivo Insulin Sensitivity by Dietary Methionine Restriction in Mice

*Diabetes* 2014;63:3721–3733 | DOI: 10.2337/db14-0464

To understand the physiological significance of the reduction in fasting insulin produced by dietary methionine restriction (MR), hyperinsulinemic-euglycemic clamps were used to examine the effect of the diet on overall and tissue-specific insulin sensitivity in mice. The steady-state glucose infusion rate was threefold higher in the MR group and consistent with the 2.5- to threefold increase in 2-deoxyglucose uptake in skeletal muscle, heart, and white adipose tissue. Dietary MR enhanced suppression of hepatic glucose production by insulin, enhanced insulin-dependent Akt phosphorylation in the liver, and increased hepatic expression and circulating fibroblast growth factor 21 (FGF-21) by fourfold. Limitation of media methionine recapitulated amplification of Akt phosphorylation by insulin in HepG2 cells but not in 3T3-L1 adipocytes or C2C12 myotubes. Amplification of insulin signaling in HepG2 cells by MR was associated with reduced glutathione, where it functions as a cofactor for phosphatase and tensin homolog. In contrast, FGF-21, but not restricting media methionine, enhanced insulin-dependent Akt phosphorylation in 3T3-L1 adipocytes. These findings provide a potential mechanism for the diet-induced increase in insulin sensitivity among tissues that involves a direct effect of methionine in liver and an indirect effect in adipose tissue through MR-dependent increases in hepatic transcription and release of FGF-21.

Normal rodent diets contain on average 5–7 g methionine and 3–4 g cysteine per kg of diet. However, a series of recent studies has shown that eliminating cysteine and

limiting dietary methionine to 1.7 g/kg produces a highly beneficial metabolic phenotype and increased longevity (1–6). The metabolic responses include reduced adiposity, reduced circulating and tissue lipid levels, increased plasma adiponectin and fibroblast growth factor 21 (FGF-21), and reduced fasting insulin and blood glucose (7–10). Reduced accumulation of adipose tissue occurs despite a hyperphagic response to the methionine-restricted (MR) diet, owing to a commensurate increase in energy expenditure that fully compensates for the increase in energy intake (6,7). The reduction in adiposity is accompanied by a change in endocrine function of adipose tissue, with increased adiponectin release and a reduction in leptin expression that is disproportionate to the reduction in adiposity (5,7,9,11). Dietary MR also increases hepatic expression and release of FGF-21 (5,12), an insulin-sensitizing hormone that promotes browning of white adipose tissue (WAT) and increases peripheral glucose uptake and utilization (13,14). In addition, FGF-21 increases adiponectin secretion from WAT (15), illustrating how the primary effects of MR in liver may have tertiary sites of action through targeted effects on endocrine function of adipose tissue.

Although specific components of the overall response to MR are initiated within hours of introduction of the diet, the full response only becomes evident over the following weeks as the cumulative effects of MR on energy balance, lipid metabolism, and endocrine function are translated into the full metabolic phenotype (16). As such, understanding the mechanistic basis for the overall phenotype involves understanding the interrelationships

Laboratory of Nutrient Sensing and Adipocyte Signaling, Pennington Biomedical Research Center, Baton Rouge, LA

Corresponding author: Thomas W. Gettys, [gettystw@pbr.c.edu](mailto:gettystw@pbr.c.edu).

Received 20 March 2014 and accepted 13 June 2014.

© 2014 by the American Diabetes Association. Readers may use this article as long as the work is properly cited, the use is educational and not for profit, and the work is not altered.

among the component responses to the diet and determining their interdependence. A critical unresolved question is how the reduction in dietary methionine is sensed and how the sensing is communicated to target sites. The specific focus of the present work is to assess the tissue-specific effects of dietary MR on insulin sensitivity and attempt to determine the basis for the previously observed improvements in glucose tolerance (11) and metabolic flexibility (7) produced by the diet. Using hyperinsulinemic-euglycemic clamps, ex vivo analysis of tissues from MR mice, and a novel in vitro model of MR, we show that dietary MR produces a significant overall increase in insulin sensitivity through a combination of direct effects on hepatic insulin signaling and indirect effects in other peripheral tissues, such as adipose tissue, by increasing hepatic expression and release of FGF-21.

## RESEARCH DESIGN AND METHODS

### Animals and Diets

Experiments conducted at the Pennington Biomedical Research Center and at Vanderbilt University were approved by the respective Institutional Animal Care and Use Committees. All experiments used male C57BL/6J mice obtained from The Jackson Laboratory (Bar Harbor, ME) at 5 weeks of age. Upon arrival, mice were adapted to the control diet for 7 days and then randomly assigned to receive the control or MR diet for 8 weeks thereafter. The feeding paradigm and diets were as described previously (6), with the control diet containing 0.86% methionine and the MR diet containing 0.17% methionine. Diets and water were provided ad libitum, room temperature was 22–23°C, and lights were on from 7 A.M. to 7 P.M.

### Experiment 1: Hyperinsulinemic-Euglycemic Clamps

One week before hyperinsulinemic-euglycemic clamps, catheters were surgically placed in the carotid artery and jugular vein for sampling and infusions, respectively. Mice were fasted for 5 h before the hyperinsulinemic-euglycemic clamp procedure, which was performed as described previously (17,18). Erythrocytes were replaced to prevent a decline in hematocrit that occurs with repeated blood sampling. A primed (1.5  $\mu\text{Ci}$ ) continuous (0.075  $\mu\text{Ci}/\text{min}$ ) [ $^3\text{H}$ ]glucose infusion was started at –20 min. The clamp was initiated at 0 min with a continuous insulin infusion (2.5 mU/kg/min) that was maintained for 145 min. Arterial glucose was measured at 10-min intervals to provide feedback to adjust the glucose infusion rate (GIR) containing [ $^3\text{H}$ ]glucose as needed to clamp glucose concentration and specific activity. [ $^3\text{H}$ ]glucose kinetics were determined at –10 min and at 10-min intervals between 80 and 120 min because insulin action is in a steady state by this interval. Plasma insulin was measured at –10, 100, and 120 min during the procedure. A 13  $\mu\text{Ci}$  intravenous bolus of [ $^{14}\text{C}$ ]2-deoxyglucose ([ $^{14}\text{C}$ ]2-DG) was administered at 120 min and used to determine the glucose metabolic index ( $R_g$ ), an indication of tissue-specific glucose uptake. Blood samples were collected at 2, 5, 10, and 25 min after injection to measure

the disappearance of [ $^{14}\text{C}$ ]2-DG from the plasma. Tissues were collected to assess tissue-specific  $R_g$ . Whole-body glucose appearance ( $R_a$ ) and endogenous glucose production (endo  $R_a$ ), a measure of hepatic glucose production, were calculated as previously described (17,18). The reader is referred to the detailed step-by-step procedure manual that is publicly accessible and maintained by the Vanderbilt Mouse Metabolic Phenotyping Center for a full description of the procedure and associated calculations ([www.mc.vanderbilt.edu/documents/mmpc/files/2012%20Lab%20Manual\(1\).pdf](http://www.mc.vanderbilt.edu/documents/mmpc/files/2012%20Lab%20Manual(1).pdf)).

### Experiment 2

Two cohorts of mice fed the respective diets for 8 weeks were studied to examine growth responses and acute in vivo signaling responses to insulin. Body weight, composition, energy intake, and energy expenditure were measured in cohort 1, as previously described (6,7). Mice in cohort 2 were fasted for 4 h before receiving intraperitoneal injections of saline or insulin (0.8 units/kg body weight). Tissues (liver, muscle, and brown adipose tissue [BAT]) were harvested from the injected animals in each dietary group after 12 min and snap frozen. Whole-cell extracts were prepared from each tissue to measure insulin-dependent phosphorylation of Akt or insulin receptor (IR) by immunoblotting. Phosphatidylinositol(3-5)-trisphosphate (PIP3) concentrations and phosphatidylinositide 3-kinase (PI3K) activity were determined using the PIP3 Mass and PI3K Activity ELISA kits (Echelon Biosciences Inc., Salt Lake City, UT). PIP3 was extracted from 100 mg frozen pulverized livers from mice fed their respective diets. Samples were run in triplicate, and data were normalized to tissue weight. PI3K was immunoprecipitated from 1 mg liver lysates using an IR substrate-1 (IRS1) antibody before assay.

To examine effects of MR on basal and insulin-dependent glucose uptake in adipose tissue, adipocytes were isolated from epididymal WAT (EWAT) and interscapular BAT depots of mice from cohort 1 in experiment 2 after 8 weeks of the control or MR diet, and [ $^3\text{H}$ ]-labeled 2-DG uptake was measured as previously described (19). In brief, isolated adipocytes were kept in glucose-free Krebs-Ringer-phosphate buffer (10 mmol/L HEPES, 125 mmol/L NaCl, 5 mmol/L KCl, 1 mmol/L  $\text{KH}_2\text{PO}_4$ , 1.25 mmol/L  $\text{CaCl}_2$ , 1.25 mmol/L  $\text{MgSO}_4$ , 2.5 mmol/L pyruvate, and 1% BSA) during the isolation and for 1 h before insulin addition. Then, adipocytes were treated with insulin for 15 min, followed by the addition of 0.1 mmol/L radiolabeled 2-DG (2  $\mu\text{Ci}/\text{mL}$ ). As a control, duplicate aliquots of cells were treated with 50  $\mu\text{mol}/\text{L}$  cytochalasin (Sigma-Aldrich, St. Louis, MO). Uptake was calculated using the ratio of counts per min (cpms) in cells per cpms added, with cpms measured in cytochalasin-treated cells subtracted from values measured in insulin treated cells. Aliquots of cells were dried on filter paper and weighed. Final uptake was normalized to dry cell weight.

### Experiment 3

To assess the direct effects of MR on enhancement of insulin signaling in liver, an *in vitro* model was developed using custom media to allow incubation of HepG2 cells with different concentrations of methionine. HepG2 cells were cultured in DMEM supplemented with 10% FBS, L-glutamine, and penicillin/streptomycin (Invitrogen, Grand Island, NY). For MR, cells were washed with PBS and normal or methionine-restricted DMEM without FBS but with L-glutamine, and penicillin/streptomycin was added. Normal DMEM contains 0.2 mmol/L methionine and L-cystine, whereas the MR medium contains only 0.01 mmol/L of each. After 18 h, the cells were incubated with increments of insulin, followed by measurement of Akt activation. To assess for potential direct effects of MR on adipocytes and muscle cells, 3T3-L1 adipocytes and C2C12 myotubes were incubated overnight with media containing various amounts of methionine, followed by incubation with vehicle or insulin and measurement of Akt activation. In some experiments, 3T3-L1 adipocytes were preincubated with 10 nmol/L FGF-21 for 5 min before measurement of Akt and Erk1/2 activation, or with 100 nmol/L FGF-21 for 24 h for 2-DG uptake experiments. The relative instability and short half-life of FGF-21 necessitated the use of higher concentrations in overnight incubations. The BIOXYTECH GSH/GSSG-412 Assay kit (Oxis Research, Portland, OR) was used to determine glutathione (GSH)/glutathione disulfide (GSSG) in HepG2 cells, following the manufacturer's protocol.

### Experiment 4

To assess the time-dependent increase in hepatic expression of FGF-21 mRNA after exposure to dietary MR, livers were harvested from mice after 12 h, 8 days, 2 weeks, and 4 weeks after the initial introduction of dietary MR. The study involved eight mice per diet per time point.

### Quantitative Real-Time PCR Analysis

Expression of FGF-21 mRNA was measured in individual tissue samples from each animal by quantitative real-time PCR, as described previously (20).

### Measurement of IR, Akt, and Erk1/2 Activation

Phosphorylation of IR, Akt, and Erk1/2 in tissues and cultured cells was measured by Western blot. Pulverized tissues and cultured cells were lysed in 10 mmol/L Tris (pH 7.4), 150 mmol/L NaCl, 1 mmol/L EDTA, 1 mmol/L EGTA, 1% Triton X-100, 0.5% NP40, protease, and phosphatase inhibitor mixes (Pierce, Thermo Fisher Scientific Inc., Rockford, IL), aspirated three times with a 20-gauge needle, and centrifuged at 10,000g for 10 min. Total protein in the extracts was measured using the Lowry method, SDS-PAGE was performed, and proteins were transferred to polyvinylidene fluoride membranes. Blots were probed with anti-phospho-IR, anti-phospho-Akt, and anti-phospho-Erk1/2 and stripped and then probed with anti-IR (total), anti-Akt (total), and anti-ERK (total). Intensity of the visualized bands was quantitated by scanning densitometry using ImageJ software.

### Antibodies and Chemicals

Antibodies to phospho-Akt (Ser473), phospho-IR (Tyr1162/1163), phosphatase and tensin homolog (PTEN), and total Akt were from Millipore (Temecula, CA), to phospho-Erk1/2 (Thr202/Tyr204) and Erk1/2 from Cell Signaling Technologies (Danvers, MA), and to IR $\beta$  and IRS1 from Santa Cruz Biotechnology (Santa Cruz, CA). Radiolabeled [1,2- $^3\text{H}$ ]-2-DG was obtained from American Radiolabeled Chemicals Inc. (St. Louis, MO). Cytochalasin and other chemicals were from Sigma-Aldrich. FGF-21 in serum was measured using an ELISA (R&D Systems, Minneapolis, MN). FGF-21 for cell culture studies was from BioVision (Milpitas, CA).

### Data Analysis

Diet-induced differences in GIR, endo R<sub>a</sub>, and tissue-specific R<sub>g</sub> in experiment 1, and insulin-dependent IR phosphorylation, Akt phosphorylation, Erk phosphorylation, and 2-DG uptake in experiments 3 and 4 were tested using a two-tailed Student *t* test, with protection set against type I errors at 5%. Differences between basal and insulin-dependent IR phosphorylation, Akt phosphorylation, PI3K activity, and PIP3 concentrations in control and MR mice in experiment 2 were compared using a two-way ANOVA, with diet and injection treatment as main effects. The diet  $\times$  injection interaction was tested using residual variance (animal within diet  $\times$  injection) as the error term, followed by post hoc testing for specific differences using the Bonferroni correction.

## RESULTS

### Hyperinsulinemic-Euglycemic Clamps

To assess the overall and tissue-specific effects of dietary MR on insulin sensitivity, hyperinsulinemic-euglycemic clamps were used after mice ate the control or MR diets for 8 weeks. Before initiating the infusion of insulin to begin the hyperinsulinemic-euglycemic clamp ( $-10$  min), fasting glucose was similar between the groups (control,  $113 \pm 3$  mg/dL; MR,  $103 \pm 6$  mg/dL) whereas insulin was significantly lower in the MR group ( $1.11 \pm 0.3$  ng/mL) compared with the control group ( $2.46 \pm 0.5$  ng/mL). After initiation of insulin infusion at time 0, blood glucose fell initially in the MR group until compensatory increases in GIR reestablished euglycemia and maintained steady-state glucose levels during the final hour of the hyperinsulinemic-euglycemic clamp (Fig. 1A). Blood glucose was stable the entire time in the control group, with the GIR needed to establish steady state reached in the first 20 min of the clamp (Fig. 1A and B). The steady-state GIR required to maintain euglycemia in the MR group was 3.1-fold higher than the GIR in the control mice (Fig. 1B). Whole-body and liver glucose metabolism was assessed using [ $^3\text{H}$ ]glucose infusion to calculate basal endo R<sub>a</sub> and compare insulin-dependent suppression of endo R<sub>a</sub> during the hyperinsulinemic-euglycemic clamp. Despite the difference in fasting insulin, basal endo R<sub>a</sub> was comparable between the groups, whereas suppression of hepatic glucose production by insulin was significantly greater in MR mice than

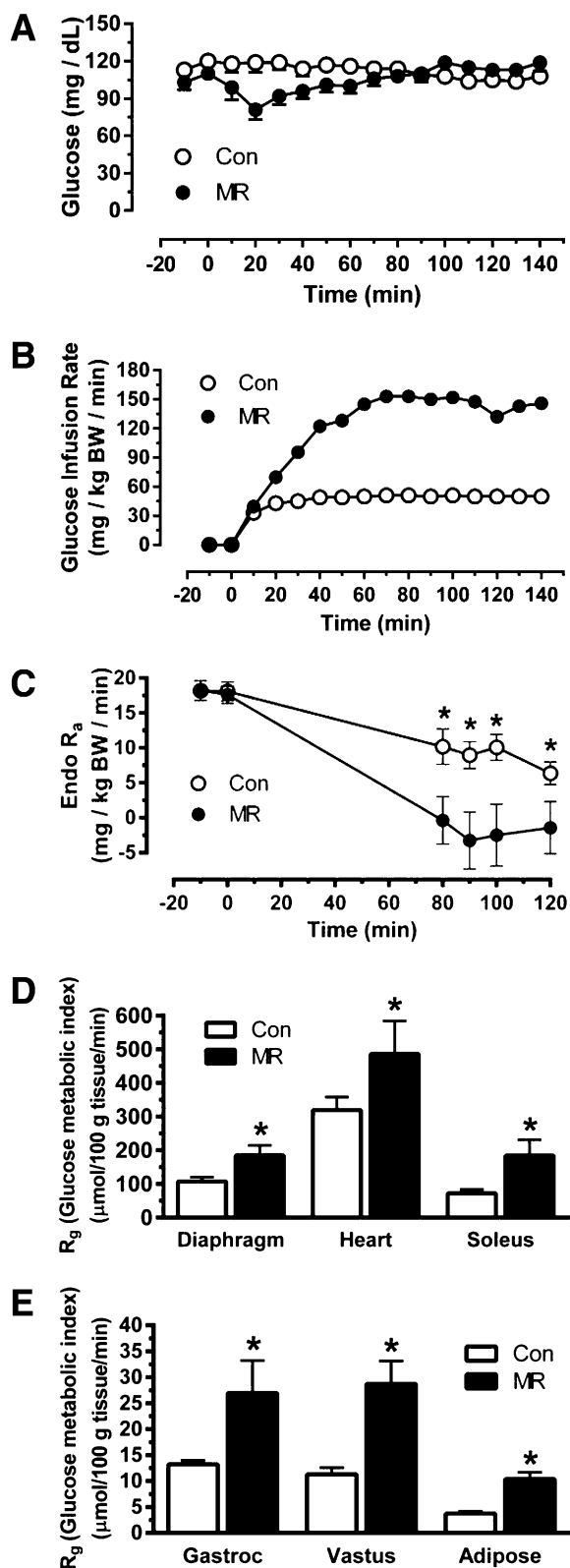


**Figure 1**—Hyperinsulinemic-euglycemic clamps in C57BL/6J mice after 8 weeks of dietary MR. The clamp procedures were conducted as described in RESEARCH DESIGN AND METHODS, and the clamp procedure was initiated at 0 min with a continuous insulin infusion (2.5 mU/kg/min) that was maintained for 140 min. Glucose was infused at a rate sufficient to maintain euglycemia until a steady-state GIR was reached. **A:** Blood glucose levels during the clamp procedure.

in controls (Fig. 1C). The  $R_g$  provides a direct measure of insulin sensitivity in each tissue, and it showed that MR produced a two- to threefold increase in uptake of [ $^{14}$ C]2-DG in diaphragm, heart, gastrocnemius muscle, soleus muscle, vastus muscle, and WAT (Fig. 1D and E). Compared with control mice, the enhanced ability of insulin to suppress hepatic glucose production and stimulate glucose uptake in peripheral tissues of MR mice was fully consistent with the observed increase in GIR that was needed to establish and maintain euglycemia during the hyperinsulinemic-euglycemic clamp in this group.

### Insulin-Dependent Akt Activation

To test for enhanced signaling efficacy as a component of enhanced insulin sensitivity, acute insulin-dependent activation of Akt was measured in liver, BAT, and skeletal muscle of mice after 8 weeks of the respective diets.

An insulin dose (0.8 units/kg body weight) was used that produced only a modest, insignificant increase in phosphorylation of hepatic Akt in control mice (Fig. 2A). In contrast, the same dose of insulin produced a threefold increase in phosphorylation of hepatic Akt in the MR group. Phosphorylation of the IR (Fig. 2B) and IRS1-bound PI3K activity (Fig. 2C) did not differ between the groups, but basal and insulin-dependent increases in PIP3 were both greater in the MR group (Fig. 2D), indicating that amplification of insulin signaling in the MR group was downstream of IR autophosphorylation and PI3K activation. Insulin-dependent Akt phosphorylation was also enhanced by MR in muscle (Fig. 2E) and BAT (Fig. 2F), showing a comparable increase of insulin-signaling efficacy in liver, muscle, and BAT. In the second cohort of mice in experiment 2, dietary MR reduced body weight by 28%, adiposity by 53%, EWAT weight by 210%, and liver weight by 25%, while increasing lean body mass by 11%, energy intake by 26%, and total energy expenditure by 25% (Table 1).

To examine MR effects on insulin signaling in adipose tissue and test for diet-induced changes in linkage to physiological responses, white and brown adipocytes were isolated and incubated with increments of insulin. Figure 3A shows that insulin-dependent phosphorylation of Akt was significantly higher in white adipocytes from MR mice compared with controls at 1 and 10 nmol/L insulin. Interestingly, basal [ $^3$ H]-2-DG uptake was higher in white adipocytes from MR compared with control mice, and insulin-dependent [ $^3$ H]-2-DG uptake was also higher in

**B:** The GIR required to maintain euglycemia during the insulin clamps. BW, body weight. **C:** Basal endo  $R_a$  and its suppression by insulin during the clamp procedure. **D** and **E:**  $R_g$ , an indication of tissue-specific insulin-dependent glucose uptake. Means  $\pm$  SEM are presented for each variable and based on  $n = 8$  for control diet and  $n = 9$  for dietary MR. \*Means differ from their corresponding controls at  $P < 0.05$ .

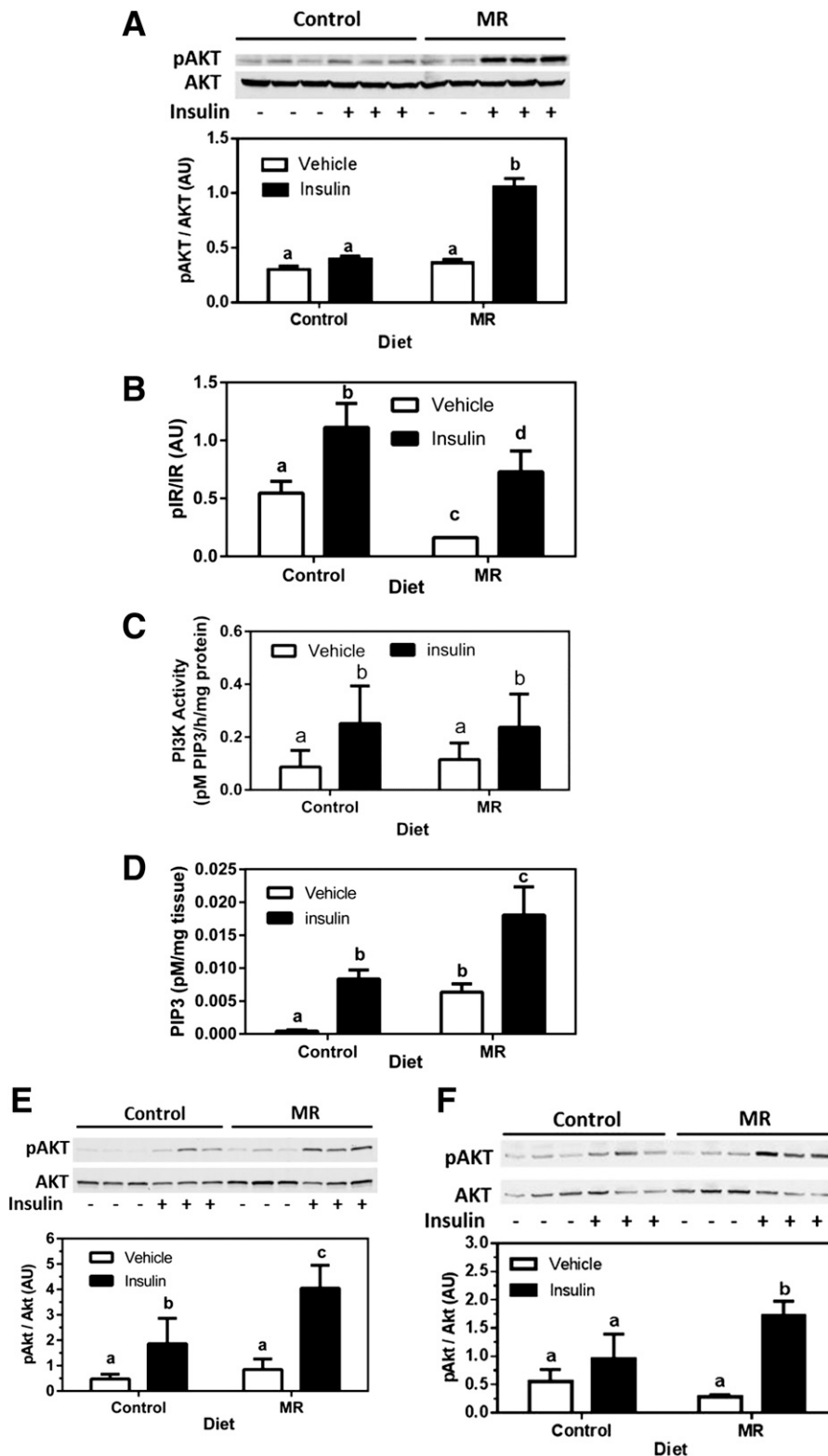


**Figure 2**—Short-term signaling responses in liver, muscle, and BAT after an acute injection of insulin in mice after 8 weeks of dietary MR. Mice fed the control or MR diets received intraperitoneal injections of saline (vehicle) or insulin (0.8 units/kg body weight) at time 0. Tissues were harvested after 12 min from the animals in each dietary group and snap frozen. Insulin-dependent phosphorylation (p) of Akt (A), IR (B), activity of IRS1-bound PI3K (C), and increases in PIP3 in liver (D). Insulin-dependent phosphorylation of Akt in gastrocnemius muscle (E) and BAT (F). Total Akt (A, E, and F) was measured as a loading control, and scanning densitometry was used to quantitate expression levels for each protein. Phosphorylated forms of each protein are expressed relative to the total. Means  $\pm$  SEM are presented for each variable and based on  $n = 6$  for control diet and  $n = 8$  for MR. Means denoted with a different letter (a, b, c, d) differ at  $P < 0.05$ .

**Table 1—Changes in body weight, adiposity, liver weight, energy intake, and energy expenditure in C57BL/6J mice after 8 weeks of dietary MR**

	Control diet	MR diet
Body weight (g) <sup>1</sup>	30.4 ± 1.5 <sup>a</sup>	23.8 ± 0.75 <sup>b</sup>
% Fat ([g fat/g BW] × 100) <sup>1</sup>	23.6 ± 1.96 <sup>a</sup>	15.4 ± 0.57 <sup>b</sup>
% Lean ([g lean/g BW] × 100) <sup>1</sup>	62.7 ± 1.81 <sup>a</sup>	69.4 ± 0.42 <sup>b</sup>
EWAT (g) <sup>1</sup>	1.26 ± 0.18 <sup>a</sup>	0.60 ± 0.05 <sup>b</sup>
Liver weight (g) <sup>1</sup>	0.99 ± 0.06 <sup>a</sup>	0.79 ± 0.05 <sup>b</sup>
Energy		
Intake (kJ/day/g BW)	2.19 ± 0.05 <sup>a</sup>	2.77 ± 0.04 <sup>b</sup>
Expenditure (kJ/mouse/h) <sup>2</sup>	1.89 ± 0.02 <sup>a</sup>	2.37 ± 0.02

BW, body weight. Means ± SEM from 8 mice per group were compared using *t* tests. <sup>a,b</sup>Means differ at *P* < 0.05. <sup>1</sup>BW, body composition, EWAT, and liver weight were measured after 8 weeks of dietary MR. Body composition was measured by nuclear magnetic resonance, and the % fat and % lean were expressed as a percentage of BW. EWAT and liver weights were measured after euthanasia, and energy intake was the average daily consumption during the course of the study. <sup>2</sup>Energy expenditure was measured in a TSE Systems Indirect Calorimetry at the end of the study. All mice were acclimated to chambers for 24 h, followed by continuous recording of O<sub>2</sub> consumption, CO<sub>2</sub> production, energy intake, and activity for 3 days at 40-min intervals. BW and composition were measured before mice entered the chambers and immediately upon exit. The energy expenditure for each mouse at each 40-min interval was calculated as previously described (7). Diet-induced differences in energy expenditure (kJ/mouse/h) were tested using ANCOVA, calculating least squares means that accounted for variation in the energy expenditure attributable to differences in lean mass, fat mass, activity, and energy intake among the mice. The least square means ± SEM for each diet were compared using *t* tests.

the MR adipocytes at all tested insulin concentrations (Fig. 3B). A similar conclusion was reached in isolated brown adipocytes, where basal and insulin-stimulated [<sup>3</sup>H]-2-DG uptake were both higher in cells isolated from MR compared with control mice (Fig. 3C). These findings are consistent with the clamp data showing a higher R<sub>g</sub> for [<sup>3</sup>H]-2-DG in adipose tissue (Fig. 1E) and extend the findings to include BAT.

#### In Vitro Model of Dietary MR

To explore cellular mechanisms for the MR-dependent increase in insulin sensitivity among tissues, custom media were used that permitted precise control of media methionine concentrations in cultured HepG2 cells, C2C12 myotubes, and 3T3-L1 adipocytes. Incremental limitation of media methionine and cysteine in HepG2 cells produced a concentration-dependent enhancement of insulin-dependent Akt phosphorylation, with maximal amplification occurring at 0.01 mmol/L methionine, which translates to a 95% restriction (Fig. 4A). The time course of insulin-dependent Akt phosphorylation was not altered by limiting media methionine, but at all points between 2 and 30 min, the activation of Akt was

significantly higher in methionine-restricted HepG2 cells (Fig. 4B). Limiting media methionine also enhanced the potency of insulin to activate Akt in HepG2 cells (Fig. 4C), similar to what was seen in the livers from MR mice (Fig. 2A). The increase in potency of insulin to activate Akt occurred without a change in autophosphorylation of the IR (Fig. 4D), indicating that the amplification of insulin signaling was downstream of the IR. In contrast to HepG2 cells, limitation of media methionine in C2C12 myotubes (Fig. 4E) or 3T3-L1 adipocytes (Fig. 4F) had no discernible effect on insulin-dependent Akt activation in either cell line. These findings establish that the insulin-sensitization response of liver cells to methionine restriction is direct and autonomous. In contrast, the results suggest that insulin sensitization by MR in muscle and adipose tissue may be indirect and not strictly dependent on limitation of methionine or cysteine to the cell. Alternatively, the failure of C2C12 myotubes and 3T3-L1 adipocytes to respond to low media methionine may be a reflection of the low capacity of muscle and adipose tissue to synthesize GSH from methionine or cysteine relative to liver (21). Therefore, caution is warranted in interpreting these findings.

#### Role of Hepatic GSH and PTEN in Insulin Signal Amplification

GSH is an essential cofactor of GSH peroxidases, which play a key role in regulating insulin-signaling intensity by regulating the activation state of protein tyrosine phosphatases such as PTEN (22–27). Because dietary MR produces a significant decrease in hepatic GSH (28,29), we tested whether in vitro MR would produce a similar decrease in cell GSH and amplify insulin signaling to Akt by limiting PTEN reactivation after treatment with H<sub>2</sub>O<sub>2</sub>. Figure 5A shows that an overnight incubation of HepG2 cells with 0.01 mmol/L methionine produced a threefold decrease in cellular GSH and a fourfold decrease in GSSG relative to control cells. In addition, a 5-min incubation of HepG2 cells with increasing concentrations of H<sub>2</sub>O<sub>2</sub> produced a concentration-dependent increase in the ratio of oxidized (inactive) to reduced (active) PTEN in both groups, but the conversion to inactive PTEN was significantly greater in HepG2 cells that had been MR overnight (Fig. 5B). More importantly, the inactivation of PTEN produced by the addition of H<sub>2</sub>O<sub>2</sub> resulted in far greater amplification of Akt phosphorylation by insulin in the MR cells compared with control cells (Fig. 5C). As before, the enhancement of insulin-dependent Akt activation was evident without addition of H<sub>2</sub>O<sub>2</sub> in MR cells, but Fig. 5C shows that addition of 50 and 200 μmol/L H<sub>2</sub>O<sub>2</sub> further enhanced amplification of insulin signaling in these cells. Because MR does not amplify IR autophosphorylation (Fig. 4D), we tested for downstream amplification and found that insulin-dependent PIP3 levels were fourfold higher in cells incubated overnight with low methionine (Fig. 5D). These findings suggest that the reduction in glutathione produced by MR in HepG2 cells limits the capacity

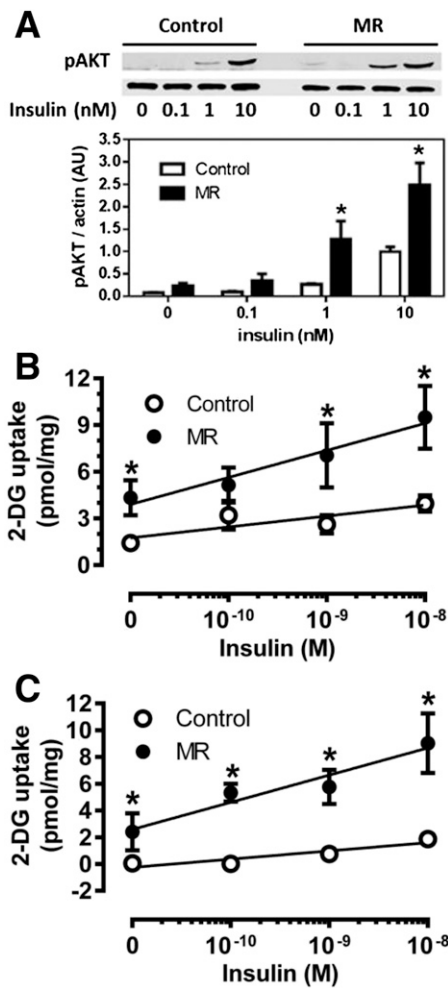


**Figure 3**—Effect of dietary MR on ex vivo insulin signaling and insulin-stimulated glucose uptake in isolated white and brown adipocytes. Epididymal white adipocytes or brown adipocytes were isolated after 8 weeks of dietary MR and incubated with increments of insulin for 5 min (Akt) or 15 min (<sup>3</sup>H]-2-DG) before measurement of Akt phosphorylation (A) and [<sup>3</sup>H]-2-DG uptake (B) in white adipocytes or [<sup>3</sup>H]-2-DG uptake in brown adipocytes (C) as described in RESEARCH DESIGN AND METHODS. Scanning densitometry was used to quantitate expression levels for each protein. Means ± SEM are representative of three independent experiments. \*Mean responses at each insulin concentration differ from their corresponding controls at *P* < 0.05.

of the cells to reactivate oxidized PTEN, resulting in amplification of insulin activation of Akt by increasing PIP3.

**Effects of MR on Hepatic Expression and Release of FGF-21**

To test the hypothesis that dietary MR enhances insulin sensitivity in adipose tissue through an indirect mechanism involving the insulin sensitizer, FGF-21, hepatic expression and release of the hormone were evaluated after 8 weeks of MR. Figure 6A shows that MR produced a threefold increase in FGF-21 mRNA that was mirrored by a fourfold increase in serum FGF-21. To examine whether increased transcription of hepatic FGF-21 is increased only after chronic exposure to MR, FGF-21 mRNA

and plasma FGF-21 were measured in mice after consumption of the diet for different times. Figure 6B shows that MR increased plasma FGF-21 and hepatic FGF-21 mRNA by 10-fold within the first 12 h of exposure to the diet. Moreover, similar increases were maintained after 1, 2, and 4 weeks’ consumption of the diet (Fig. 6B).

To test for acute effects of FGF-21 on adipocyte insulin sensitivity, 3T3-L1 adipocytes were incubated with FGF-21 for 5 min, followed by 5 additional min with increments of insulin. As reported previously (30), FGF-21 preincubation increased basal Erk1/2 phosphorylation compared with vehicle and also modestly amplified insulin-dependent Erk1/2 phosphorylation (Fig. 6C). The effect of FGF-21 on Erk1/2 activation was subtle but consistent across all insulin concentrations (Fig. 6C), confirming the biological activity of the FGF-21 used in these studies. In contrast to Erk1/2, the effect of FGF-21 on Akt phosphorylation was not evident in the absence of insulin, but in cells incubated with 10 nmol/L insulin, Akt phosphorylation was threefold higher in adipocytes preincubated with FGF-21 compared with vehicle (Fig. 6D). Overnight incubation with FGF-21 also enhanced basal and insulin-dependent 2-DG uptake in 3T3-L1 adipocytes (Fig. 6E), similar to what was seen in isolated adipocytes from MR mice (Fig. 3B). Collectively, these findings are consistent with the hypothesis that dietary MR is enhancing insulin sensitivity in nonhepatic tissues in part by inducing the expression and release of the insulin sensitizer, FGF-21, from the liver.

**DISCUSSION**

Selective dietary MR produces a highly integrated series of behavioral, physiological, and biochemical responses that improve biomarkers of metabolic health and increase longevity in rodents (1,3,7–9,31,32). In the present work, we provide definitive evidence that dietary MR increases overall insulin sensitivity by threefold and tissue-specific insulin sensitivity in the liver, skeletal muscle, heart, and adipose tissue by two- to threefold. A schematic illustrating the proposed mechanisms through which dietary MR enhances peripheral insulin sensitivity is provided in Fig. 7. We propose that insulin sensitivity is increased in part by increasing hepatic transcription and release of FGF-21, which enhances insulin-dependent signaling and glucose uptake. In addition, the evidence shows that dietary MR increases steady-state levels of PIP3 after IR activation by affecting its degradation but not its synthesis. This occurs because reduced dietary methionine limits the formation of cysteine, an essential precursor of hepatic GSH. The reduction of GSH limits GSH-sensitive degradation of PIP3 by PTEN, which enhances PIP3-dependent activation of Akt (Fig. 7).

The uniformity of the enhancement of insulin sensitivity across tissues suggests several potential mechanisms, none of which necessarily excludes the others, because some combination of mechanisms seems quite likely. The overall improvement was not surprising, given

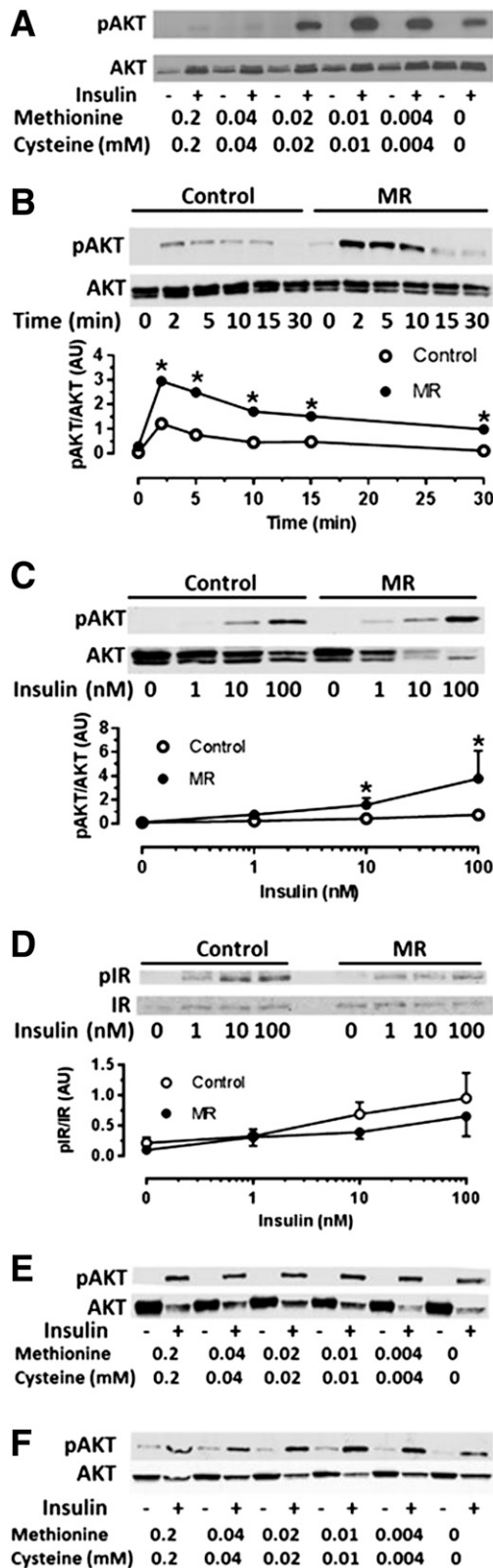


**Figure 4**—Insulin-dependent phosphorylation (p) of Akt or IR in cultured HepG2 cells (A–D), C2C12 cells (E), and 3T3-L1 adipocytes (F) after incubation in media containing normal concentrations or increments of MR as described in RESEARCH DESIGN AND METHODS. A: HepG2 cells were incubated for 18 h with the indicated concentrations of methionine and cysteine, followed by incubation with 10 nmol/L insulin for 5 min and measurement of Akt

the wide-ranging improvements in metabolic status produced by the diet. For example, previous work using indirect calorimetry to evaluate the effects of MR on substrate utilization provided compelling evidence that the MR diet enhanced metabolic flexibility and increased glucose utilization during the fed state (6,7). Together, these findings raise the central question of how sensing of reduced methionine is translated into an organism-wide improvement in insulin sensitivity.

One attractive hypothesis is that diet-induced changes in lipid metabolism, adiposity, and release of insulin-sensitizing hormones from adipose tissue and the liver produce the improvement. Under this scenario, one could argue that the primary effect of MR is on energy balance and that secondary benefits accrue in large measure from reduced adiposity and associated reductions in circulating and tissue lipids. For example, short-term calorie restriction reduces adiposity and plasma lipids and increases plasma levels of the insulin-sensitizing hormone, adiponectin, by twofold (7). In long-term studies with ad libitum and pair-fed control rats (11), the MR diet produced a twofold greater reduction in adiposity and an increase in adiponectin than found in the pair-fed controls but a fourfold greater reduction in fasting insulin. These findings support the view that reductions in adiposity resulting from MR contribute to improved insulin sensitivity but also suggest that MR produces additional improvements not explained solely by its effects on energy balance. Although adiponectin is a potential mediator of the effects of MR on insulin sensitivity, studies with adiponectin-null mice indicate that adiponectin is not essential to the decrease in adiposity or to the increase in glucose tolerance produced by the diet (authors' unpublished results). However, a limitation of these studies is that the diet-induced reduction in adiposity may have obscured the contribution of adiponectin to the response.

The rapid and persistent increase in MR-dependent hepatic transcription and release of FGF-21 (Fig. 6A and B) suggests an additional mechanism through which MR may be acting to increase insulin sensitivity in peripheral tissues. Recent studies make a compelling case that FGF-21 is a powerful metabolic regulator in the context of glucose and lipid homeostasis, producing a wide range

phosphorylation by Western blotting. B: Time-dependent phosphorylation of Akt in HepG2 cells in response to 10 nmol/L insulin after 18 h of incubation of cells with control levels (0.2 mmol/L) or restricted levels (0.01 mmol/L) of methionine and cysteine. Insulin concentration-dependent Akt phosphorylation (C) or IR phosphorylation (D) in HepG2 cells after culturing for 18 h in control (0.2 mmol/L) or restricted levels (0.01 mmol/L) of methionine and cysteine. Insulin-dependent Akt phosphorylation in C2C12 myotubes (E) or 3T3-L1 adipocytes (F) after 18 h of incubation in indicated concentrations of methionine and cysteine. Phosphorylated Akt or IR was expressed relative to total Akt or total IR. Means  $\pm$  SEM are representative of three independent experiments. \*Mean responses at each insulin concentration differ from their corresponding controls at  $P < 0.05$ .

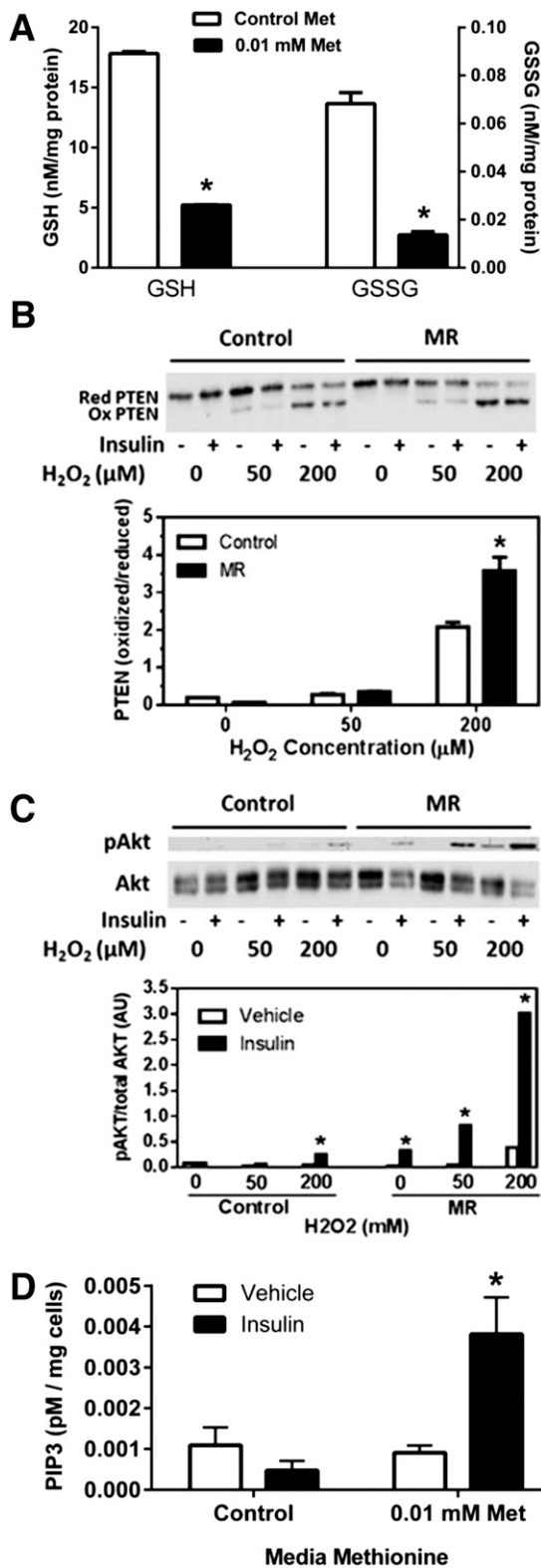


**Figure 5**—Lowering of reduced GSH and oxidized GSSG levels and amplification of insulin-dependent phosphorylation of Akt by oxidation of PTEN with H<sub>2</sub>O<sub>2</sub> in HepG2 cells cultured for 18 h in control (0.2 mmol/L) or restricted levels (0.01 mmol/L) of methionine (Met) and cysteine. **A**: After 18 h of incubation under these conditions, GSH and GSSG levels were measured in whole-cell extracts of HepG2 cells. Additional HepG2 cells were incubated for 5 min with 0, 50, or 200 μmol/L H<sub>2</sub>O<sub>2</sub> in the absence and presence of

of beneficial metabolic changes (14,30,33–37). These biological responses were cataloged in studies where FGF-21 was infused at high doses or increased via transgenes. Therefore, it is unclear whether the normal 1.5- to two-fold induction of FGF-21 produced by fasting or ketogenic diets (38,39) is sufficient to elicit the metabolic responses observed in pharmacological interventions (40). Our findings show that dietary MR produces a persistent increase in plasma FGF-21 to nearly 5 ng/mL (Fig. 6A), which is a fourfold induction and two- to threefold higher than increases produced by fasting and ketogenic diets (39). Moreover, many—if not most—of the metabolic, transcriptional, and signaling effects attributed to FGF-21 are fully reproduced by dietary MR (7,8,12). For example, FGF-21 directly affects adiponectin secretion from adipocytes (15), increases lipogenic gene expression in WAT (33), promotes browning of WAT (41), and increases thermogenic gene expression in BAT and WAT (41). Dietary MR produces significant browning of WAT (7,8), and given the increased glucose uptake and utilization associated with browning (42), it is attractive to suggest that MR is functioning through this mechanism to increase insulin sensitivity in WAT.

FGF-21 also acts centrally to regulate metabolism and increase energy expenditure (34,36). We have shown that dietary MR increases core temperature, energy expenditure, and thermogenic function of BAT and WAT through increases in sympathetic nervous system (SNS) stimulation of adipose tissue (6,7). That the thermogenic response of adipose tissue to cold exposure involves an SNS-dependent increase in glucose uptake, lipogenesis, and β-oxidation is well established (43,44). Therefore, it seems plausible that MR, through a combination of SNS- and FGF-21-dependent mechanisms, is affecting the observed increases in basal and insulin changes in adipose tissue through a combination of direct and central nervous system-dependent mechanisms. Alternatively, the browning of WAT and associated increase in glucose uptake could be primarily the result of MR-dependent SNS stimulation and not dependent on FGF-21. However, the direct enhancement of insulin-dependent Akt activation by FGF-21 (Fig. 6D) suggests a contributing role of FGF-

10 nmol/L insulin. **B**: The ratio of oxidized (Ox) to reduced (Red) PTEN was visualized by Western blotting, and a representative blot of three experiments is shown. Oxidized and reduced PTEN were quantitated by densitometry and expressed as a ratio. **C**: The effect of increments of H<sub>2</sub>O<sub>2</sub> on insulin-dependent phosphorylation of Akt. Phosphorylated (p)Akt was expressed relative to total Akt. **D**: HepG2 cells were incubated for 18 h in control (0.2 mmol/L) or restricted levels (0.01 mmol/L) of methionine and cysteine, followed by incubation with 10 nmol/L insulin for 5 min and harvest of cells for measurement of PIP3. Means are from four replicates in two experiments. \*Means ± SEM differ from their corresponding controls at *P* < 0.05.

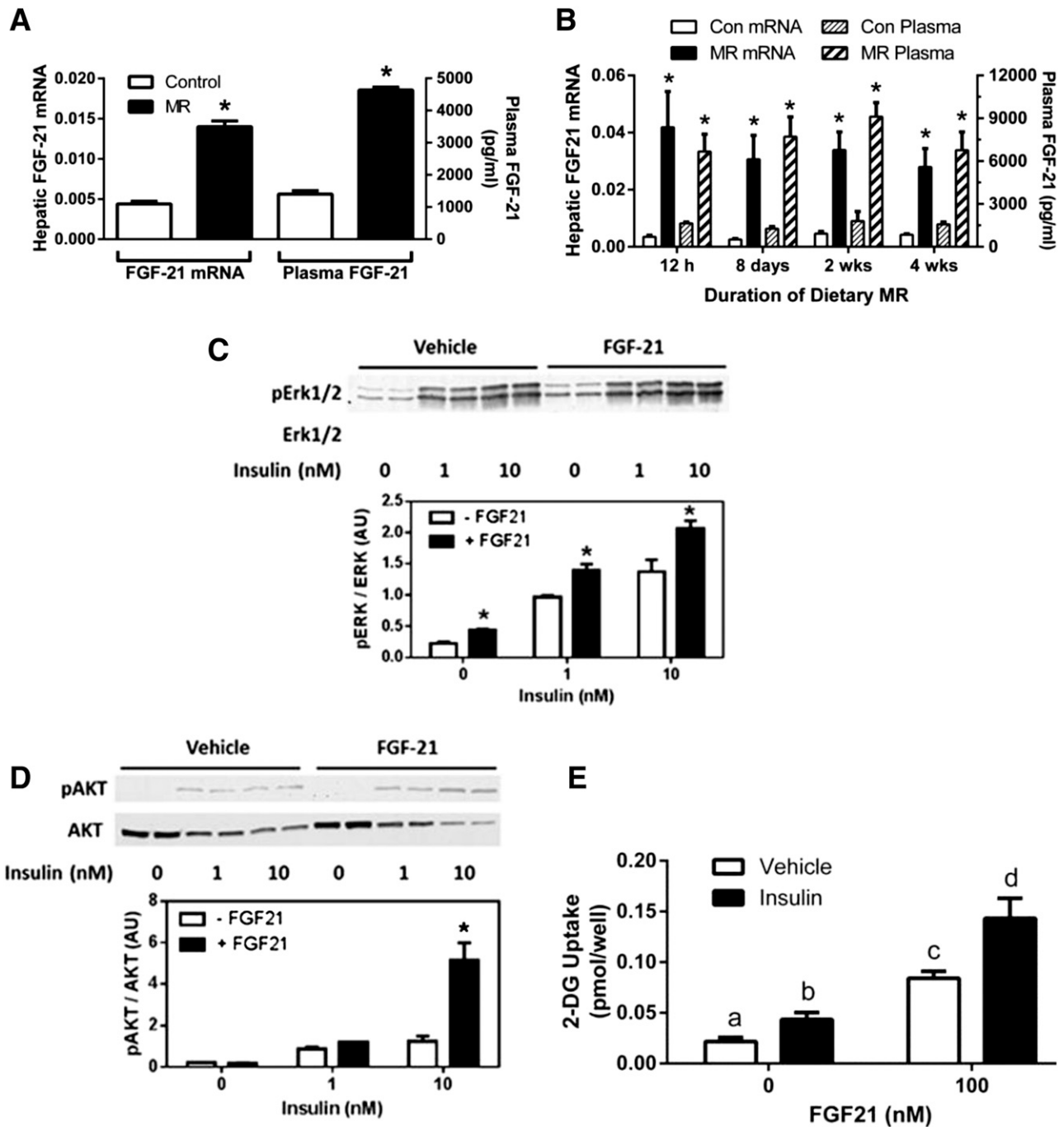


**Figure 6**—The effect dietary MR on hepatic expression and plasma levels of FGF-21 after 8 wks (A), the time-dependent change in hepatic expression of FGF-21 mRNA and plasma FGF-21 after initial exposure to MR (B), and the in vitro effect of FGF-21 on insulin-dependent phosphorylation (p) of Erk1/2 (C), Akt (D), and glucose uptake in 3T3-L1 adipocytes (E). A: Plasma FGF-21 levels and hepatic FGF-21 mRNA levels in mice after 8 weeks of dietary MR. Means  $\pm$  SEM are representative of eight mice per group. \*Means differ from their respective controls at  $P < 0.05$ . B: Time-dependent changes in hepatic FGF-21 mRNA and plasma levels in mice after initial introduction of MR. Means  $\pm$  SEM are representative of eight animals per diet per time point. \*Means differ from their corresponding control at that time point at  $P < 0.05$ . C and D: Differentiated 3T3-L1 adipocytes were treated with 10 nmol/L FGF-21 for 5 min, followed by treatment with vehicle, 1 nmol/L, or 10 nmol/L insulin for 5 additional min. Insulin-dependent phosphorylation of Erk1/2 (C) or Akt (D) was measured by Western blotting. Phosphorylated Erk1/2 and Akt were expressed relative to total Erk1/2 and Akt. Means  $\pm$  SEM are representative of three independent experiments. \*Means at each time point differ from their corresponding controls at  $P < 0.05$ . E: Differentiated 3T3-L1 adipocytes were treated with 100 nmol/L FGF-21 for 24 h, followed by treatment with vehicle or 100 nmol/L insulin for 2 h before measurement of [ $^3$ H]-2-DG uptake over the final 1 h. Means  $\pm$  SEM are representative of three independent experiments. Means denoted with a different letter (a, b, c, d) differ at  $P < 0.05$ .

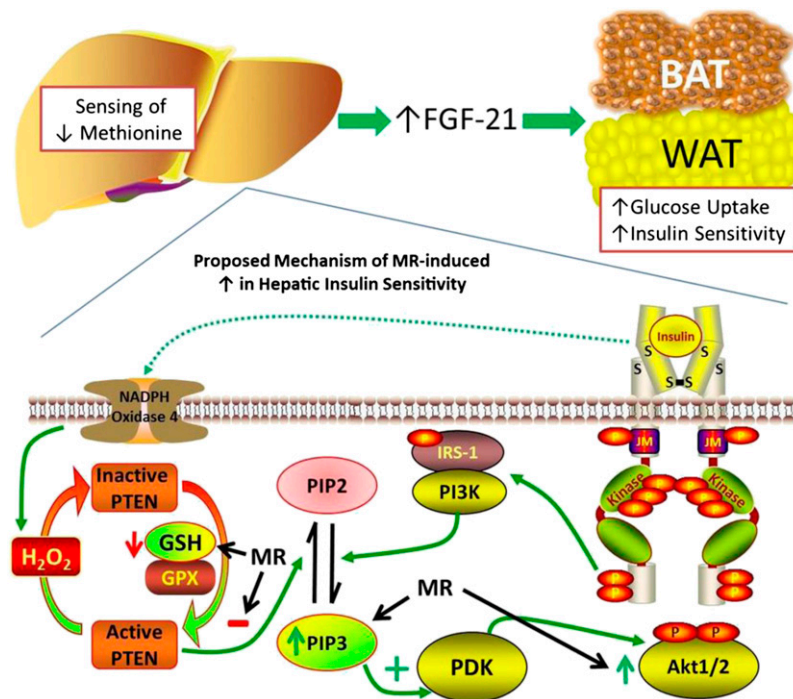


**Figure 7**—Schematic model of proposed mechanism for increase in insulin sensitivity in adipose tissue and the liver produced by dietary MR. PDK, phosphoinositide-dependent kinase. S denotes sulfur atoms involved in disulfide linkages that establish the secondary structure of the insulin receptor.

21. Future experiments with FGF-21-null mice will be important in assessing the importance of FGF-21 as a mediator of MR's biological effects on energy balance and insulin sensitivity.

The rapid increase in hepatic FGF-21 after initiation of dietary MR (Fig. 6B) supports the view that the liver is a key initial site for sensing and responding to dietary MR. Our *in vitro* recapitulation of enhanced insulin signaling in MR HepG2 cells further supports this view and provides compelling evidence that the methionine-sensitive step is mechanistically linked to the amplification of insulin signaling. The cell-autonomous nature of the response suggests two potential mechanisms. The first involves the protein kinase, general control of nonderepressible 2 (GCN2), which phosphorylates eukaryotic initiation factor 2 $\alpha$  (eIF2 $\alpha$ ) when activated by insufficient transfer RNA charging by essential amino acids. The phosphorylation of eIF2 $\alpha$  triggers a cascade of signaling events and transcriptional responses collectively referred to as the amino acid response (16). Although there is suggestive evidence that GCN2 activation by MR is linked to transcriptional repression of lipogenic genes (45), there is no indication that GCN2 activation enhances insulin signaling.

The second potential mechanism involves the reduction of hepatic GSH produced by dietary MR (29) and restriction of media methionine concentrations in HepG2 cells (Fig. 5A). Insulin-dependent activation of NADPH oxidases produces an acute increase in intracellular H<sub>2</sub>O<sub>2</sub> that temporarily inactivates protein tyrosine

phosphatases, including PTEN, by oxidizing the cysteine in their active site (24–27). PTEN and other protein tyrosine phosphatases are reactivated by reducing the oxidized cysteine in the active site, and this reactivation step is catalyzed by GSH-dependent peroxidases (22–24). We have shown that PTEN is more fully converted to its oxidized form by H<sub>2</sub>O<sub>2</sub> in HepG2 cells after MR (Fig. 5B) and that insulin-dependent phosphorylation of Akt is amplified under these conditions (Fig. 5C). PTEN dephosphorylates PIP3 formed by PI3K, so a more prolonged inactivation of PTEN by MR should result in higher PIP3 and Akt phosphorylation. This is precisely what is observed *in vivo* (Fig. 2A and D) and *in vitro* (Fig. 5D). Therefore, we hypothesize that dietary MR amplifies insulin-dependent Akt phosphorylation in the liver by reducing GSH synthesis and limiting the rate of GSH-dependent reactivation of PTEN. For a given concentration of insulin, this results in higher PIP3 levels and greater Akt phosphorylation. Collectively, our findings provide a potential mechanism for the diet-induced increase in insulin sensitivity among tissues that involves a direct effect of methionine in the liver to amplify insulin signaling and an indirect effect in adipose, and perhaps other tissues, through MR-dependent increases in hepatic release of the insulin sensitizer, FGF-21, into the circulation.

**Acknowledgments.** The authors acknowledge the excellent technical assistance of Kelly Dille, Alicia Pierce, and Mollye Baker in the Laboratory of

Nutrient Sensing and Adipocyte Signaling, Pennington Biomedical Research Center (Baton Rouge, LA) and the clerical support of Cindi Tramonte, Laboratory of Nutrient Sensing and Adipocyte Signaling, Pennington Biomedical Research Center (Baton Rouge, LA).

**Funding.** This work was partly supported by American Diabetes Association 1-12-BS-58 and 7-13-MI-05 (T.W.G.), National Institutes of Health (NIH) DK-096311 (T.W.G.) and 1F32-DK-098918-01 (D.W.), and the Vanderbilt Mouse Metabolic Phenotyping Center (NIH DK-059637). This work also made use of the Genomics and the Cell Biology & Bioimaging core facilities supported by NIH P20-GM-103528 (T.W.G.) and P30-DK-072476.

**Duality of Interest.** No potential conflicts of interest relevant to this article were reported.

**Author Contributions.** K.P.S., D.W., and T.W.G. contributed to the writing and editing of the manuscript. D.W., M.O., and C.C.C. conducted the animal experiments. K.P.S., D.W., M.O., and C.C.C. conducted the in vitro cell culture studies, the associated Western blots, and the metabolite measurements. T.W.G. analyzed the data used to produce illustrations. T.W.G. is the guarantor of this work and, as such, had full access to all the data in the study and takes responsibility for the integrity of the data and the accuracy of the data analysis.

## References

- Orentreich N, Matias JR, DeFelice A, Zimmerman JA. Low methionine ingestion by rats extends life span. *J Nutr* 1993;123:269–274
- Richie JP Jr, Leutzinger Y, Parthasarathy S, Malloy V, Orentreich N, Zimmerman JA. Methionine restriction increases blood glutathione and longevity in F344 rats. *FASEB J* 1994;8:1302–1307
- Miller RA, Buehner G, Chang Y, Harper JM, Sigler R, Smith-Wheelock M. Methionine-deficient diet extends mouse lifespan, slows immune and lens aging, alters glucose, T4, IGF-I and insulin levels, and increases hepatocyte MIF levels and stress resistance. *Aging Cell* 2005;4:119–125
- Sun L, Sadighi Akha AA, Miller RA, Harper JM. Life-span extension in mice by preweaning food restriction and by methionine restriction in middle age. *J Gerontol A Biol Sci Med Sci* 2009;64:711–722
- Ables GP, Perrone CE, Orentreich D, Orentreich N. Methionine-restricted C57BL/6J mice are resistant to diet-induced obesity and insulin resistance but have low bone density. *PLoS ONE* 2012;7:e51357
- Plaisance EP, Henagan TM, Echlin H, et al. Role of  $\beta$ -adrenergic receptors in the hyperphagic and hypermetabolic responses to dietary methionine restriction. *Am J Physiol Regul Integr Comp Physiol* 2010;299:R740–R750
- Hasek BE, Stewart LK, Henagan TM, et al. Dietary methionine restriction enhances metabolic flexibility and increases uncoupled respiration in both fed and fasted states. *Am J Physiol Regul Integr Comp Physiol* 2010;299:R728–R739
- Hasek BE, Boudreau A, Shin J, et al. Remodeling the integration of lipid metabolism between liver and adipose tissue by dietary methionine restriction in rats. *Diabetes* 2013;62:3362–3372
- Perrone CE, Mattocks DA, Hristopoulos G, Plummer JD, Krajcik RA, Orentreich N. Methionine restriction effects on 11-HSD1 activity and lipogenic/lipolytic balance in F344 rat adipose tissue. *J Lipid Res* 2008;49:12–23
- Perrone CE, Mattocks DA, Jarvis-Morar M, Plummer JD, Orentreich N. Methionine restriction effects on mitochondrial biogenesis and aerobic capacity in white adipose tissue, liver, and skeletal muscle of F344 rats. *Metabolism* 2010;59:1000–1011
- Malloy VL, Krajcik RA, Bailey SJ, Hristopoulos G, Plummer JD, Orentreich N. Methionine restriction decreases visceral fat mass and preserves insulin action in aging male Fischer 344 rats independent of energy restriction. *Aging Cell* 2006;5:305–314
- Ghosh S, Wanders D, Stone KP, Van NT, Cortez CC, Gettys TW. A systems biology analysis of the unique and overlapping transcriptional responses to caloric restriction and dietary methionine restriction in rats. *FASEB J* 2014;28:2577–2590
- Muise ES, Souza S, Chi A, et al. Downstream signaling pathways in mouse adipose tissues following acute in vivo administration of fibroblast growth factor 21. *PLoS ONE* 2013;8:e73011
- Kharitonov A, Shiyanova TL, Koester A, et al. FGF-21 as a novel metabolic regulator. *J Clin Invest* 2005;115:1627–1635
- Lin Z, Tian H, Lam KS, et al. Adiponectin mediates the metabolic effects of FGF21 on glucose homeostasis and insulin sensitivity in mice. *Cell Metab* 2013;17:779–789
- Anthony TG, Morrison CD, Gettys TW. Remodeling of lipid metabolism by dietary restriction of essential amino acids. *Diabetes* 2013;62:2635–2644
- Ayala JE, Bracy DP, McGuinness OP, Wasserman DH. Considerations in the design of hyperinsulinemic-euglycemic clamps in the conscious mouse. *Diabetes* 2006;55:390–397
- Berglund ED, Li CY, Poffenberger G, et al. Glucose metabolism in vivo in four commonly used inbred mouse strains. *Diabetes* 2008;57:1790–1799
- Tanti JF, Cormont M, Grémeaux T, Le Marchand-Brustel Y. Assays of glucose entry, glucose transporter amount, and translocation. *Methods Mol Biol* 2001;155:157–165
- Prpic V, Watson PM, Frampton IC, Sabol MA, Jezek GE, Gettys TW. Differential mechanisms and development of leptin resistance in A/J versus C57BL/6J mice during diet-induced obesity. *Endocrinology* 2003;144:1155–1163
- Stipanuk MH. Sulfur amino acid metabolism: pathways for production and removal of homocysteine and cysteine. *Annu Rev Nutr* 2004;24:539–577
- Kim Y, Song YB, Kim TY, et al. Redox regulation of the tumor suppressor PTEN by glutathione. *FEBS Lett* 2010;584:3550–3556
- Kwon J, Lee SR, Yang KS, et al. Reversible oxidation and inactivation of the tumor suppressor PTEN in cells stimulated with peptide growth factors. *Proc Natl Acad Sci U S A* 2004;101:16419–16424
- Meng TC, Buckley DA, Galic S, Tiganis T, Tonks NK. Regulation of insulin signaling through reversible oxidation of the protein-tyrosine phosphatases TC45 and PTP1B. *J Biol Chem* 2004;279:37716–37725
- Lee SR, Yang KS, Kwon J, Lee C, Jeong W, Rhee SG. Reversible inactivation of the tumor suppressor PTEN by H2O2. *J Biol Chem* 2002;277:20336–20342
- Goldstein BJ, Mahadev K, Wu X. Redox paradox: insulin action is facilitated by insulin-stimulated reactive oxygen species with multiple potential signaling targets. *Diabetes* 2005;54:311–321
- Loh K, Deng H, Fukushima A, et al. Reactive oxygen species enhance insulin sensitivity. *Cell Metab* 2009;10:260–272
- Perrone CE, Mattocks DA, Plummer JD, et al. Genomic and metabolic responses to methionine-restricted and methionine-restricted, cysteine-supplemented diets in Fischer 344 rat inguinal adipose tissue, liver and quadriceps muscle. *J Nutrigenet Nutrigenomics* 2012;5:132–157
- Richie JP Jr, Komninou D, Leutzinger Y, et al. Tissue glutathione and cysteine levels in methionine-restricted rats. *Nutrition* 2004;20:800–805
- Adams AC, Coskun T, Rovira AR, et al. Fundamentals of FGF19 & FGF21 action in vitro and in vivo. *PLoS ONE* 2012;7:e38438
- Elshorbagy AK, Valdivia-Garcia M, Mattocks DA, et al. Cysteine supplementation reverses methionine restriction effects on rat adiposity: significance of stearyl-coenzyme A desaturase. *J Lipid Res* 2011;52:104–112
- Wanders D, Ghosh S, Stone KP, Van NT, Gettys TW. Transcriptional impact of dietary methionine restriction on systemic inflammation: relevance to biomarkers of metabolic disease during aging. *Biofactors* 2014;40:13–26
- Coskun T, Bina HA, Schneider MA, et al. Fibroblast growth factor 21 corrects obesity in mice. *Endocrinology* 2008;149:6018–6027
- Holland WL, Adams AC, Brozinick JT, et al. An FGF21-adiponectin-ceramide axis controls energy expenditure and insulin action in mice. *Cell Metab* 2013;17:790–797
- Xu J, Stanislaus S, Chinookoswong N, et al. Acute glucose-lowering and insulin-sensitizing action of FGF21 in insulin-resistant mouse models—association with liver and adipose tissue effects. *Am J Physiol Endocrinol Metab* 2009;297:E1105–E1114
- Bookout AL, de Groot MH, Owen BM, et al. FGF21 regulates metabolism and circadian behavior by acting on the nervous system. *Nat Med* 2013;19:1147–1152

37. Xu J, Lloyd DJ, Hale C, et al. Fibroblast growth factor 21 reverses hepatic steatosis, increases energy expenditure, and improves insulin sensitivity in diet-induced obese mice. *Diabetes* 2009;58:250–259
38. Adams AC, Kharitonov A. FGF21: The center of a transcriptional nexus in metabolic regulation. *Curr Diabetes Rev* 2012;8:285–293
39. Badman MK, Pissios P, Kennedy AR, Koukos G, Flier JS, Maratos-Flier E. Hepatic fibroblast growth factor 21 is regulated by PPARalpha and is a key mediator of hepatic lipid metabolism in ketotic states. *Cell Metab* 2007;5:426–437
40. Angelin B, Larsson TE, Rudling M. Circulating fibroblast growth factors as metabolic regulators—a critical appraisal. *Cell Metab* 2012;16:693–705
41. Fisher FM, Kleiner S, Douris N, et al. FGF21 regulates PGC-1 $\alpha$  and browning of white adipose tissues in adaptive thermogenesis. *Genes Dev* 2012;26:271–281
42. Emanuelli B, Vienberg SG, Smyth G, et al. Interplay between FGF21 and insulin action in the liver regulates metabolism. *J Clin Invest* 2014;124:515–527
43. Inokuma K, Ogura-Okamatsu Y, Toda C, Kimura K, Yamashita H, Saito M. Uncoupling protein 1 is necessary for norepinephrine-induced glucose utilization in brown adipose tissue. *Diabetes* 2005;54:1385–1391
44. Yu XX, Lewin DA, Forrest W, Adams SH. Cold elicits the simultaneous induction of fatty acid synthesis and beta-oxidation in murine brown adipose tissue: prediction from differential gene expression and confirmation in vivo. *FASEB J* 2002;16:155–168
45. Dudek SM, Semenkovich CF. Essential amino acids regulate fatty acid synthase expression through an uncharged transfer RNA-dependent mechanism. *J Biol Chem* 1995;270:29323–29329